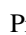



Quantum half-orphans in kagome antiferromagnets

Pranay Patil ¹, Fabien Alet,¹ Sylvain Capponi ¹ and Kedar Damle²

¹Laboratoire de Physique Théorique, Université de Toulouse, CNRS, UPS, France

²Department of Theoretical Physics, Tata Institute of Fundamental Research, Mumbai 400005, India



(Received 24 September 2020; accepted 8 December 2020; published 28 December 2020)

We numerically study the effects of nonmagnetic impurities (vacancies) in the spin- S Heisenberg antiferromagnet on the kagome lattice. For a range of low but nonzero temperatures, and spin values that extend down to $S = 2$, we find that the magnetization response to an external magnetic field is consistent with the response of emergent “half-orphan” degrees of freedom that are expected to dominate the response of the corresponding classical magnet in a similar temperature range whenever there are two vacancies on the same triangle. Specifically, for all spin values we have considered (from $S = 1/2$ to 4), there is a large enhancement of the local susceptibility of the lone spin on such a triangle with two vacancies; in the presence of a uniform magnetic field h , this lone-spin behaves effectively as an almost free spin S in an effective field $h/2$. Quite remarkably, in the zero-temperature limit, the ground state in the presence of a half-orphan has a nonzero total spin value S_{GS} that shows a trend similar to $S/2$ when $S \geq 2$. These qualitative aspects of the response differ strikingly from the more conventional response of diluted samples without such half-orphan degrees of freedom. We discuss how these findings could be checked experimentally.

DOI: [10.1103/PhysRevResearch.2.043425](https://doi.org/10.1103/PhysRevResearch.2.043425)

I. INTRODUCTION

The low-temperature physics of frustrated quantum magnets is controlled by the interplay between the geometric frustration, quantum fluctuations, entropic effects, and quenched disorder. In many interesting cases [1], the geometric frustration renders the leading exchange interactions unable to drive magnetic ordering even at temperatures much lower than the scale of these interactions. Instead, in a semiclassical picture, they confine the system to a manifold of minimally frustrated configurations, which can admit a description in terms of emergent degrees of freedom as in the case of classical spin ice [2]. The low-temperature physics is then controlled by how these emergent degrees of freedom behave in the presence of subdominant interactions as well as quantum and thermal fluctuations. In the extreme quantum limit, frustrated $S = 1/2$ magnets can provide an arena for the physics of quantum number fractionalization, the Majorana fermion excitations of Kitaev’s honeycomb model being a celebrated example [3].

Interestingly, quenched disorder, i.e., nonmagnetic substitutional impurities or lattice imperfections that affect the bond strengths in their vicinity, can provide a powerful probe of these emergent excitations and their unusual quantum numbers. For instance, the emergent magnetic monopole excitations of classical spin ice can be nucleated in the ground state of a disordered sample. Similarly, vacancies in Kitaev’s

honeycomb model nucleate a Majorana fermion- Z_2 flux complex in their vicinity. More generally, a wide variety of features can be probed or created by nonmagnetic impurities in magnetic systems, depending on the nature of the underlying state. If the clean system is a spin liquid, then nonmagnetic impurities can lead to spinon deconfinement [4] or even spin-charge separation if they are mobile [5]. More conventional ordering patterns can also be characterized by the response to nonmagnetic impurities [6]. An enhancement of local correlations is often observed near spinless impurities in antiferromagnets [7]. In valence bond crystals that break lattice symmetries, or valence bond solids that are nondegenerate, nonmagnetic impurities generically induce a localized spin texture around them [4]. In systems with competing phases at low temperatures, nonmagnetic impurities can furthermore reveal or seed competing orders [8]. Quantum critical systems have also been shown [9,10] to host responses characteristic of their criticality to the inclusion of spinless defects. All these different physical behaviors and the corresponding local textures or responses have been detected in magnetic compounds using local probe techniques, such as nuclear magnetic resonance (NMR). Let us mention, for instance, the spin “polaron” observed in the two-dimensional doped material, $\text{SrCu}_2(\text{BO}_3)_2$ [11,12]; the imaging of spin-1/2 edge excitations in the spin-1 Haldane compound $\text{Y}_2\text{BaNi}_{1-x}\text{Mg}_x\text{O}_5$ [13]; the magnetic response around an impurity observed in an $S = 1/2$ kagome compound (herbertsmithite) [14]; and the localized bound states generated by impurities in topological magnets [15].

Coming back to frustrated magnets, the $\text{SrCr}_9\text{pGa}_{12-9\text{p}}\text{O}_{19}$ (SCGO) compound, in which Cr^{3+} $S = 3/2$ moments lie on the vertices of the pyrochlore-slab (bilayer kagome) lattice, provides another striking example of the interplay between

Published by the American Physical Society under the terms of the [Creative Commons Attribution 4.0 International license](https://creativecommons.org/licenses/by/4.0/). Further distribution of this work must maintain attribution to the author(s) and the published article’s title, journal citation, and DOI.

impurities and the underlying physical state [16–18]. Even in the best samples of SCGO, nonmagnetic Ga atoms disrupt the corner-sharing network of triangles and tetrahedra formed by the Cr ions; these Ga impurities can be modeled as static vacancies in the Heisenberg antiferromagnet on this lattice. At a classical level, the Heisenberg model on the pyrochlore slab lattice remains disordered down to $T = 0$, providing an interesting example of a classical spin liquid with full $SU(2)$ symmetry of interactions [19,20].

Following an earlier phenomenological analysis [21] of experimental results on SCGO, Henley [22] described the $T = 0$ liquid state in terms of an emergent fluctuating polarization field and noted that a triangle with two vacancies led to a lone or “orphan” spin on that triangle, which behaves as a source (charge) for this polarization field. The polarization field of this charge leads, in this description, to an oscillating spin texture with a power-law envelope. Even without a detailed computation of this texture, this effective theory predicts that the classical spin- S Heisenberg model on the pyrochlore slab lattice will have a net spin polarization of $S/2$ in the direction of an infinitesimal external magnetic field at $T = 0$.

Motivated by this factor of 2, which is suggestive of *spin fractionalization*, Henley dubbed this combination of the lone spin and the resulting spin-texture a “half-orphan,” modifying the terminology of “orphan spins” introduced in the earlier phenomenological studies [21]. In closely related work [19] that studied the classical Heisenberg antiferromagnet on the pyrochlore and pyrochlore-slab lattices, Moessner and Berlinsky also recognized the special role of these half-orphan degrees of freedom in dominating the low-temperature magnetic response, and they used this insight to model the experimental results on SCGO with varying degrees of dilution. These results were achieved using a single-unit approximation where the properties of individual simplices were taken as input.

This striking $T = 0$ prediction of a saturation magnetization of $S/2$ for the system with two vacancies on the same triangle led immediately to the following questions: Does the low-temperature susceptibility show signatures of this “spin fractionalization”? In other words, does the impurity susceptibility of this orphan-texture complex correspond to that of a classical spin- $S/2$ object? If yes, how is this response resolved spatially? Motivated by these questions, Ref. [23] used a hybrid large- N field-theory as well as direct Monte Carlo simulations to study the low but nonzero temperature behavior. Perhaps surprisingly, the answer turns out to be in the affirmative, with an interesting spatial structure that will be important in our present study: At low temperatures T in the spin-liquid regime, each lone spin on a triangle with two vacancies “sees” an effective magnetic field that has magnitude $h/2$ (where h is the applied external field) and responds to it as a free spin S in this field at temperature T . Exactly half of this paramagnetic response is canceled off by the net diamagnetic response of the surrounding spin texture for which this orphan spin serves as a source, giving rise to a net susceptibility that equals the susceptibility of a spin $S/2$ at temperature T .

In conjunction with subsequent work [24] that also characterized the entropic interactions between these half-orphan degrees of freedom, this approach provides a fairly detailed picture of both the orphan-texture complex and its

susceptibility, as well as interactions between orphans, including a theory for low-temperature glassy behavior in the multi-orphan case. Importantly, it provides a reasonably satisfactory fit to NMR data on SCGO [18,25] that could not previously be accounted for by more conventional ideas. We provide more details on orphan physics in the classical case in the Appendix for completeness, along with classical Monte Carlo simulations for kagome systems, as starting from now we will focus on kagome planes (and not bilayers).

While one expects that the classical physics of half-orphans would be reflected in some form in a semiclassical treatment of the corresponding quantum magnet with large but finite spin S , this expectation has thus far not been shored up by an actual controlled calculation of $1/S$ corrections to the classical picture. Nor has the fairly impressive success of classical descriptions of $S = 3/2$ frustrated magnets such as SCGO been quantitatively examined from this point of view.

Spin $S = 1/2$ kagome magnets such as herbertsmithite [26,27] also feature some degree of dilution by nonmagnetic vacancies. Since it is well known that the classical kagome magnet has a fairly broad low-temperature spin-liquid regime, extending upward from a lower cutoff of $T^* \sim 10^{-3}JS^2$ (that marks a subtle crossover to an ordered regime below this temperature [28–30]), one expects that half-orphans seeded by vacancy-pairs should be fairly well-defined at the classical level in this regime. These observations provide the central motivation for the present study, in which we ask the following: Do these emergent half-orphan degrees of freedom nucleated by pairs of vacancies on the same triangle survive quantum effects in the Heisenberg antiferromagnet on the kagome lattice?

The presence of nonmagnetic impurities in some of the best-known experimental realizations of frustrated quantum magnets on the kagome lattice has motivated several studies of vacancy effects, which we build on here with our work. For instance, a single nonmagnetic impurity is known to induce local dimer order in the spin-1/2 case [31], and it does not generate a localized spin in the spin-3/2 case either [32], while a finite concentration could lead to valence bond glass in the spin-1/2 case [33]. Using a combination of series expansion and variational wave-function studies, Gregor and Motrunich [34] have also modeled inhomogeneous Knight shifts in compounds such as Herbertsmithite [26] by studying the response of the $S = 1/2$ kagome antiferromagnet to nonmagnetic impurities. Again, there is no evidence that single vacancies induce the kind of dramatic enhancement that pairs of vacancies do in the classical picture.

In this paper, we study the finite-temperature as well as ground-state signatures of orphan physics in the spin- S quantum Heisenberg model on the kagome lattice for a large set of spin values ranging from $S = 1/2$ up to $S = 6$, allowing us to discuss the quantum to classical crossover. One striking result of our study is that the ground state of the quantum system with two vacancies on the same triangle has nonzero spin quantum number S_{GS} . This tracks $[S/2]$, which is the total quantum spin value (allowed to exist in the system) which is the closest to $S/2$, i.e., we find $S_{GS} \simeq [S/2]$ down to $S = 2$. This provides a dramatic quantum manifestation of half-orphan physics at $T = 0$. In some way, this result is reminiscent of the $S = 1/2$ end-spins in cut $S = 1$ Haldane gap

chains, which provide the clearest and most experimentally relevant signature of the underlying symmetry-protected topological order in these systems. However, this is qualitatively different: The presence of quantum half-orphans in the ground state of samples with two vacancies on the same triangle is blind to the integer or half-integer nature of elementary spin S , and is perhaps best thought of as a semiclassical effect that survives to surprisingly low values of S . Indeed, there is no obvious underlying topological order at the heart of this effect.

In our finite-temperature studies, we find that the local susceptibility offers a very clear signature of orphan physics down to $S = 2$. We attribute this to the presence of quantum half-orphans in the ground state of these systems. From other probes such as the magnetization curve, we find that orphan physics can be detected to even lower values of quantum spin (down to $S = 1/2$), with specific signatures not present for other types of impurity patterns. We also present an analysis of the histogram of spin magnetization due to a distribution of impurities, akin to a NMR Knight shift experiment, specific to the experimentally relevant $S = 1/2$ situation. Our results are obtained with a finite-temperature method working in Krylov bases generated by an appropriate number of randomly distributed initial states (see details below), as well as Lanczos exact diagonalization (ED) and density matrix renormalization group (DMRG) for the study of ground-state properties.

The layout of this paper is as follows: In Sec. II we first study the $T = 0$ ground state and present our results on the ground-state polarization, as well as spin textures obtained through ED and DMRG computations. We begin Sec. III with a brief description of the finite-temperature random sampling technique used to simulate thermodynamics of the quantum system, and then we present finite-temperature results for orphan physics, including the local susceptibility response, the magnetization curve, as well as experimental predictions for the NMR Knight shift. Finally, Sec. IV summarizes our results along with a discussion of some outstanding issues. For completeness, in the Appendix we also present the results of finite-temperature Monte Carlo simulations of vacancy effects in the classical Heisenberg model on the kagome lattice, and we identify the temperature regime in which orphan physics is clearly visible in the classical case.

II. GROUND-STATE PHYSICS IN THE QUANTUM CASE

We begin with perhaps the simplest question that gets to the heart of the intriguing conundrum posed by Henley, Moessner, and Berlinksy's *classical* $T = 0$ argument for a saturation magnetization of $S/2$ that reflects the presence of a half-orphan nucleated by two vacancies on a triangle: What is the ground-state spin quantum number of a spin- S quantum antiferromagnet on a kagome lattice with two vacancies on one triangle of the lattice?

To answer this question for the kagome magnet with Hamiltonian

$$H = \sum_{\langle i,j \rangle} \vec{S}_i \cdot \vec{S}_j, \tag{1}$$

we first compute the total spin of the ground-state for some of the lattices shown in Fig. 1. This is done using Lanczos exact diagonalization for kagome samples with an orphan spin, up

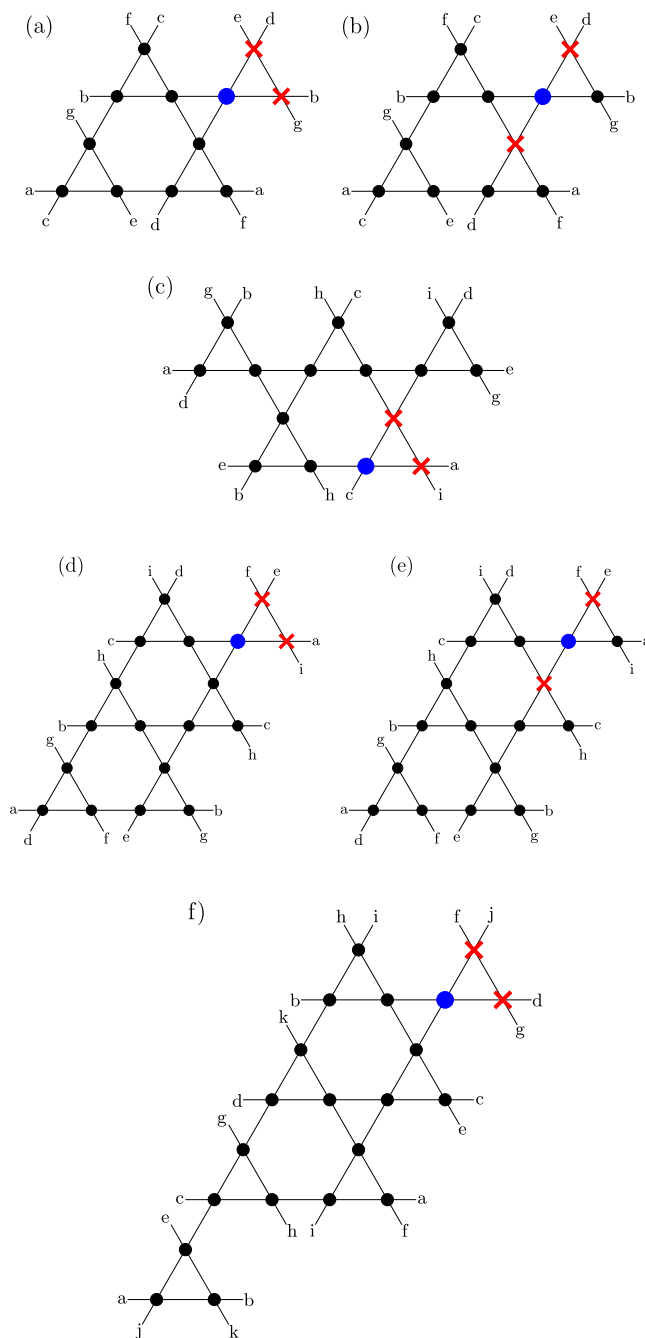


FIG. 1. Kagome lattices with N sites and two nonmagnetic impurities (denoted as red crosses). Periodic boundary conditions are shown through system-spanning bonds denoted by alphabetical indices. (a), (c), (d), and (f) Samples with $N = 12, 15, 18,$ and 21 sites, respectively, for which the positions of the impurities create an orphan spin (denoted as a blue dot). (b) and (e) Samples with $N = 12$ and 18 where the impurities are next-nearest neighbors and do *not* create an orphan spin. The blue dot in those cases denotes the spin which we monitor for the magnetization or local susceptibility in Sec. III.

to $S = 6$. This is represented in Fig. 2, where we find that starting from $S \geq 2$, the ground state is no longer a singlet. We compare the total spin S_{GS} of the ground state to $S/2$ (dashed line in Fig. 2), and we find an overall trend toward

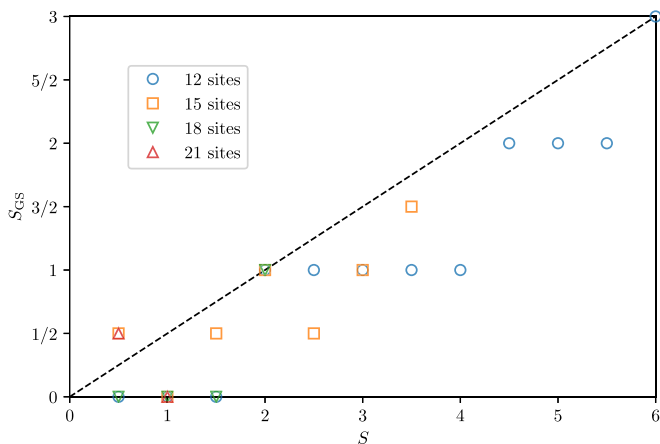


FIG. 2. Ground-state global spin S_{GS} as a function of local spin- S for kagome lattices of varying sizes with an orphan spin. The straight line is the classical prediction $S_{GS} = S/2$.

this classical prediction. In particular, the ground-state spin S_{GS} tracks in most cases the (half-)integer closest to $S/2$ which is allowed in the sample. The results in Fig. 2 are mostly for the 12-site samples with a pair impurity, but we find the same for the few larger clusters that we are able to simulate. In particular, we find $S_{GS} = 1$ for spin-2 lattices of sizes 15 and 18 with an orphan impurity. We were able to check also a combination of spin and lattice size where the global total spin is half-integer $\in \{1/2, 3/2, 5/2, \dots\}$. Note, for instance, the case of $S = 7/2$ spins on a 15-site sample with a pair impurity (13 sites effective) where we find that $S_{GS} = 3/2$, which is indeed the allowed value closest to the classical prediction.

These results should be contrasted with all other cases we have tested, such as the pure case and different arrangements of the impurities (for one or two nonmagnetic impurities). In these more conventional configurations, we always find the ground state to be of the lowest possible spin (a global singlet $S_{GS} = 0$ when the total number of spins is even). This is consistent with what is expected for conventional antiferromagnets.

In addition to this, we also study the ground-state texture for cases in which it is not a global singlet. This can be done by calculating $\langle S_i^z \rangle$ for all sites on the lattice in the highest polarized state in the ground-state multiplet. This is shown explicitly in Fig. 3 for $S = 11/2$. Since the ground state has total spin $S_{GS} = 2$ (see Fig. 2), we have measured the distribution of magnetization in the $S_{total}^z = \sum_{i=1}^N S_i^z = 2$ sector. There is clearly a larger effect at the orphan site that tapers off with increasing distance, but due to the relative small size of the lattice, other sites are affected as well.

In Fig. 4, we present other magnetization profiles for much larger system sizes using DMRG simulations [35–37]. We have chosen a spin $S = 2$ so that the ground state is polarized and we measure the local $\langle S_i^z \rangle$ values in the $S_{total}^z = 1$ ground state. Typically, we have kept up to $m = 8000$ states [using only $U(1)$ quantum number corresponding to the conservation of S^z] to achieve a discarded weight below 5×10^{-5} . As is often used in such simulations, we have chosen cylinder geometries, i.e., periodic boundary conditions in the short direction and open ones in the other. From these plots, it is

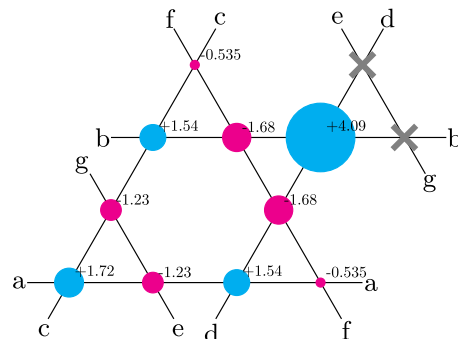


FIG. 3. Ground-state texture $\langle S_i^z \rangle$ for $S = 11/2$ measured on the highest polarized state of the ground-state multiplet, with $S_{GS} = 2$, obtained from ED for a 12-site lattice (periodic boundary conditions are indicated with identical letters), with two impurities shown as crosses. Radii of the circles are proportional to the $\langle S_i^z \rangle$ value; blue and red correspond to positive and negative values, respectively.

clear that the spin texture is well localized around the orphan spin. Moreover, the numerical values found in these larger clusters are within 10% of the ones obtained by ED on a much smaller 12-site cluster with two impurities.

To make contact with experiments, we now move to the finite-temperature regime to see if signatures of orphan spins remain and how to characterize them.

III. THERMODYNAMICS FOR THE QUANTUM VERSION

In this section, we study the thermodynamics of the quantum version of the Heisenberg model in Eq. (1) for various values of the spin S ranging from $S = 1/2$ up to $S = 4$, on samples of the kagome lattice containing one or several nonmagnetic impurities, some of which are depicted in Fig. 1.

While a full computation of the thermodynamic properties does require the complete set of eigenvalues (to get the partition function), or even eigenstates (to compute observables), it has been known for a long time that finite-temperature properties can be approximated using only a few well-chosen pure states in the correct energy window, as done in the finite-temperature Lanczos method [38]. This is rooted at the foundations of statistical mechanics since a pure state with energy E of a large system has the same local properties as a thermodynamic mixed state at the related temperature. These ideas have been put on more rigorous grounds over the years, and are known as quantum typicality [39–42].

In most of our results, we thus use a typicality scheme based on the exact application of the Hamiltonian to a random initial vector $|v_0\rangle$. Rather than using a power method with repeated applications of the Hamiltonian [43,44] which has a slower convergence, we use the formulation in the Krylov basis $\text{Span}\{|v_0\rangle, H|v_0\rangle, H^2|v_0\rangle, \dots, H^m|v_0\rangle\}$, and we choose m large enough (typically between 100 and 500) such that at least two of the lowest energy states are converged. We found that this criterion implies large enough Krylov spaces to ensure convergence at the lower temperature. Several previous works show that these approaches are particularly successful to study thermodynamic properties of frustrated magnets on lattices larger than those available with full diagonalization methods [45–48], and we refer to them for details about this

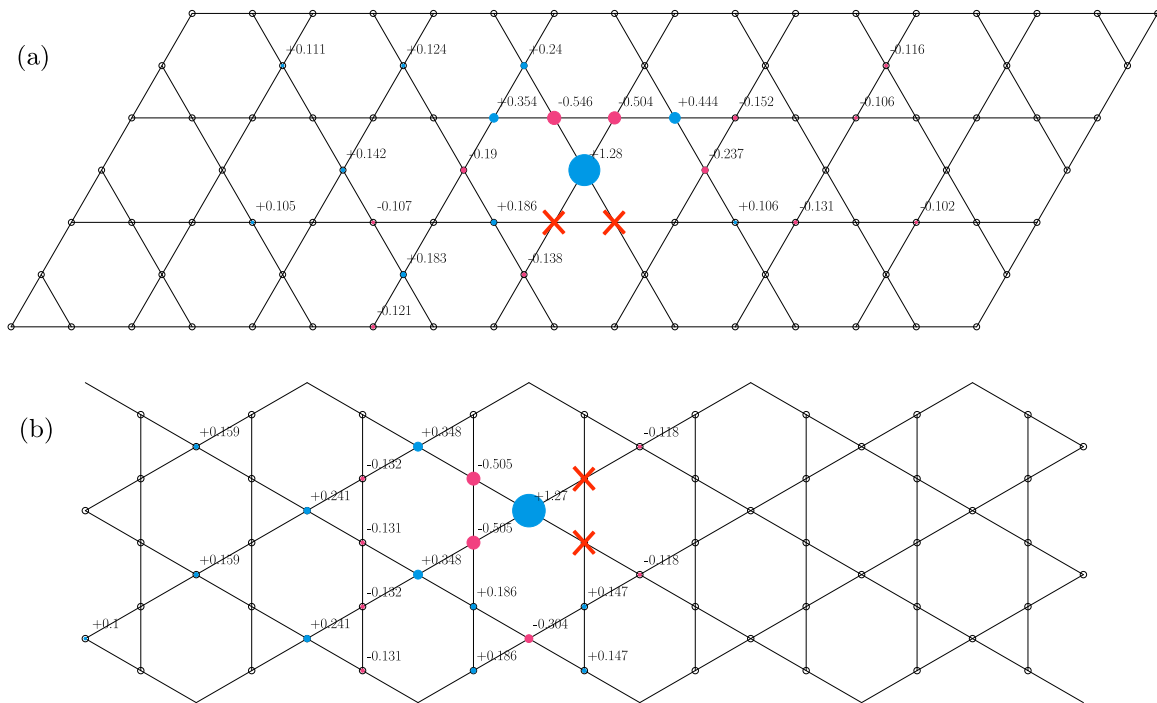


FIG. 4. Ground-state texture $\langle S_i^z \rangle$ for $S = 2$ measured in the $S_{\text{total}}^z = 1$ sector, achieved using DMRG for (a) a 6×17 lattice; and (b) a 4×19 lattice with a different orientation. Open/periodic boundary conditions are used in the long/short direction. The two crosses denote the positions of the two impurities, whereas the radius of circles and nearby numbers denote $\langle S_i^z \rangle$ (values are only shown when the absolute value is larger than 0.1).

method. Despite using exact (machine precision) application of H , all the data presented using this technique present error bars, which results from averaging over a finite number of initial random vectors $|v_0\rangle$. In our simulations, we use between 100 and 800 initial random vectors, depending on the system size, which is quite a high number (see the discussion in Ref. [49], which averages over 100 initial states). The error bars are computed using standard jackknife techniques to correctly take into account the important correlations between the numerator and denominators in all thermal expectations values [49,50].

Specific aspects of our computations are as follows: (i) the presence of impurities implies the absence of translation symmetries (for some impurity patterns, a reflection symmetry is still present), (ii) we measure expectation values of observables (such as the orphan magnetization S_{orphan}^z) that do not commute with H , hence requiring to store all Krylov vectors [47]. Even though we use total magnetization S_{total}^z conservation and spin inversion $S_i^z \rightarrow -S_i^z$ symmetry, the first point implies very large Hilbert spaces, especially for large spin S values. The second point implies a much larger memory requirement than for most applications of the typicality method which deal with observables that commute with the Hamiltonian. We mitigate this by storing all Krylov vectors in parallel for the largest samples. Both computationally demanding points limit the typicality method to kagome samples with a relatively small number of spins. We can nevertheless reach samples with up to $N = 25$ spins for $S = 1/2$ and up to $N = 10$ spins for $S = 4$.

In the following, we will present results for the total susceptibility of the sample $\chi_{\text{tot}} = \langle (S_{\text{total}}^z)^2 \rangle / T$, the local

susceptibility, defined as (see, e.g., [34]) $\chi_{\text{loc}} = \langle S_{\text{orphan}}^z S_{\text{total}}^z \rangle / T$, or the magnetization curve $S_{\text{orphan}}^z(h)$. Here S_{orphan}^z is the magnetization at an orphan site.

A. Local susceptibility

We compute the magnetic response of the spin closest to nonmagnetic impurities: it is in most cases the orphan spin [such as in Figs. 1(a), 1(c), 1(d), and 1(f)], but we also consider the closest spin for other impurity patterns [such as in Figs. 1(b) and 1(e)]. Motivated by the classical expectations outlined in the Introduction, we study the local susceptibility as a sensitive probe of orphan physics.

We compare in particular in Fig. 5 the local susceptibility of the orphan spin for the 12-site kagome sample with a pair of impurities [Fig. 1(a)] for various values of spin S to the classical result. To provide a simple comparison, we scale $T \rightarrow T/S(S + 1)$ and $1/(\chi_{\text{loc}}T) \rightarrow S(S + 1)/(\chi_{\text{loc}}T)$, in analogy with the classical case. We find an agreement between the classical version for a range of temperatures lying between a (spin-dependent) minimum temperature and arbitrarily large temperatures. The inset of Fig. 5 allows us to identify the dependence on the spin S of the typical temperature scale above which the local susceptibility is almost indistinguishable from the classical response. As expected, this temperature decreases with increasing spin S , but note that it does so even when rescaled by $S(S + 1)$. More strikingly, we find that for $S \geq 2$, the inverse local susceptibility $S(S + 1)/(\chi_{\text{loc}}T)$ appears to converge to a finite value (around $\sim 7-10$, depending on S), relatively close to that of the classical case (6 in theory, around ~ 5.5 for the 12-site samples,

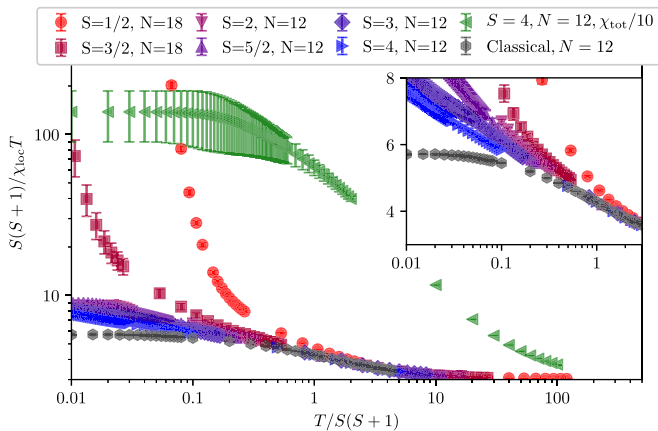


FIG. 5. Scaled inverse local susceptibility at the orphan spin site for different values of the spin- S . A comparison to the average susceptibility per site for $S = 4$ for the 12-site lattice with a pair impurity is shown. This is calculated by normalizing the total susceptibility by number of spins. Inset: magnified version where variations between different spin values can be clearly seen.

as shown in the Appendix). The lower spin values ($S = 1/2$ and $3/2$), for which we can use a larger 18-site sample, depart earlier from the classical case (as expected), the major difference lying at low temperatures where the inverse response $S(S + 1)/(\chi_{loc}T)$ diverges. Clearly, this difference has its origins in the fact that the ground state for these cases does not host a half-orphan, i.e., it is a spin singlet and does not lie in the total spin sector $S_{GS} \simeq [S/2]$.

A clear signature of the orphan spin is found by comparing its local (inverse) susceptibility to the averaged (inverse) susceptibility per site, also represented for $S = 4$ in Fig. 5: as is readily seen in this figure, the orphan spin is approximately an order of magnitude more sensitive to magnetic field at low temperatures. This is justified by assuming that a large portion of the magnetic response of the entire system is provided by the orphan spin, implying that the averaged susceptibility is $1/N$ times the orphan susceptibility, where N is the number of spins (10 in this case). It is important to understand whether this signature is unique to the orphan spin, or if it could also be found for spins close to the nonmagnetic impurities for other impurity patterns. To answer this question, we study two other kinds of impurities: (i) a single site impurity, and (ii) two impurities on neighboring plaquettes [this case corresponds to Figs. 1(b) and 1(e)].

For the former case, we consider the local susceptibility of any spin close to the impurity, while for the latter we consider the spin in between the two impurities [blue dot in Figs. 1(b) and 1(e)]. The corresponding three scaled inverse local susceptibilities are represented in Fig. 6 for $S = 2$ (representative of the generic $S \geq 2$ case) as well as for $S = 1/2$. In both cases, we find the magnetic response to be significantly stronger for the orphan spin for low to medium [$T \approx S(S + 1)$] temperatures.

The spin-1/2 case is of special importance for several compounds [26,51–53], for which local magnetic responses can be probed by NMR. Motivated by this, we study in more detail the $S = 1/2$ case for a larger variety of sample sizes

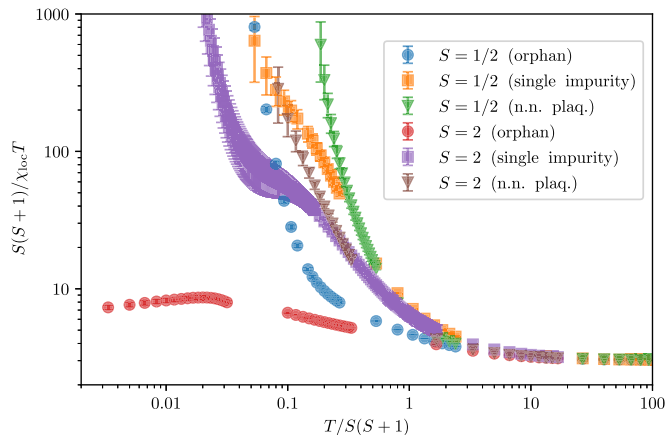


FIG. 6. Comparison between the scaled inverse local susceptibility for the orphan spin situation and other impurity patterns, for $S = 2$ on a 12-site sample and $S = 1/2$ on an 18-site sample.

and impurity patterns. In Fig. 7, we study the orphan spin configuration for an 18-site kagome sample (with effectively 16 spins), a 21-site sample (19 spins effective), and a 27-site sample with two orphan spins that are maximally separated (23 spins effective), as well as the same 27-site sample with impurities on neighboring plaquettes (25 sites effective). All of these configurations are shown in Figs. 1 and 12. When the number of spins is even, the ground state can be and is a global singlet. This feature is absent in all other cases with an odd number of spins, leading to a divergence in χ_{loc} at low temperatures. Besides the lattice-independent behavior in the high-temperature range, we observe a clear distinction in the local response between the orphan spin and other spins close to impurities, before the low-temperature signal (dominated by the ground-state nature) eventually appears. For the case of the lattice with two orphan impurities, both orphans are chosen to be equivalent from the perspective of lattice geometry, and we

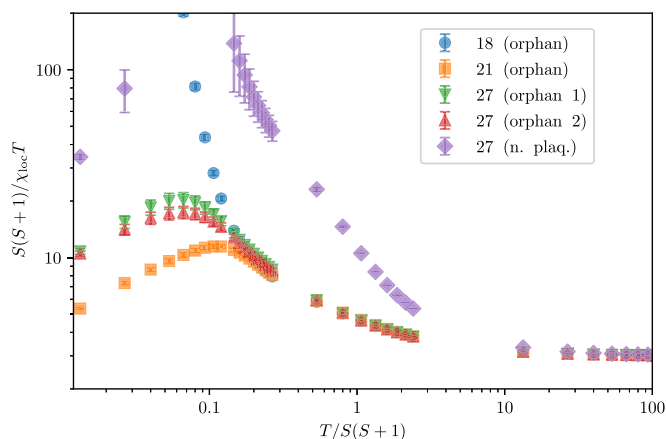


FIG. 7. Scaled inverse local susceptibility comparisons of the orphan spin for $S = 1/2$ on various samples of large sizes. For the 27-site sample, we consider two situations: one with two orphan spins (for which we distinguish the response) and one with impurities on neighboring plaquettes.

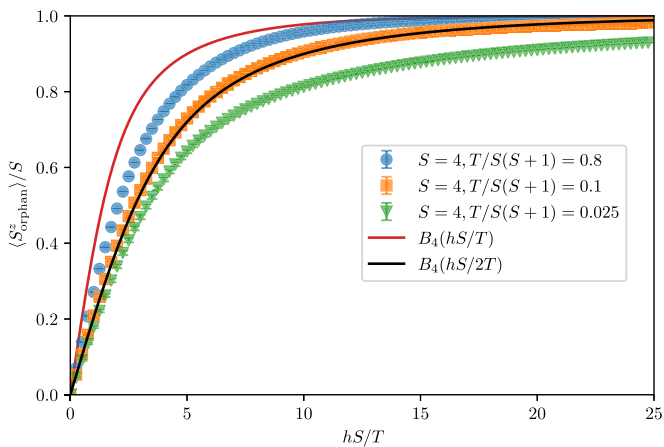


FIG. 8. Scaled orphan magnetization curve $\langle S_{\text{orphan}}^z \rangle / S$ as a function of scaled applied field hS/T at different temperatures, for a spin $S = 4$, 12-site kagome sample. The continuous curves are Brillouin functions at fields $h/2$ and h .

expect that they should have identical behavior, which is what we observe within error bars.

B. Orphan magnetization curve and effects of the screening cloud

Another important feature of orphan physics which is important to test for in the quantum case is the effect of the screening cloud on the orphan spin itself. As discussed in the Introduction, in the classical case the cloud screens half of the applied magnetic field, implying that the orphan spin responds like a free spin S in a magnetic field $h/2$. This description should work only in the temperature range where quantum and thermal effects are not strong, i.e., in an intermediate temperature range with respect to JS^2 , the coupling value.

Figure 8 displays a comparison between the scaled magnetization curve of the orphan spin $\langle S_{\text{orphan}}^z(h, T) \rangle / S$ for the spin $S = 4$ kagome 12-site sample for three different temperatures, and it compares it to the expected Brillouin functions for the full-field $B_S(hS/T)$ or half-field $B_S(hS/2T)$, where

$$B_S(x = hS/T) = \frac{2S+1}{2S} \coth\left(\frac{2S+1}{2S}x\right) - \frac{1}{2S} \coth\left(\frac{x}{2S}\right)$$

is the response to a magnetic field h of a free spin- S at temperature T . We find good agreement between the typicality data and the half-field response for a temperature $T/[S(S+1)] \approx 0.1$, and expected deviations at low and high temperature. We discuss below how to quantify the temperature scale for which the agreement is the best. We find similar behavior for lower spins, all the way down to spin- $1/2$.

In particular, motivated by the specific signature of the orphan local susceptibility in Fig. 7, we also study the field-dependent response of the orphan impurity complexes at different temperatures for the low-spin case $S = 1/2$. Once again, we find a temperature range where the screening cloud of the orphan provides a net cancellation of half the magnetic field, making the response of the orphan spin consistent with a free spin- S in a magnetic field $h/2$. This can be observed in

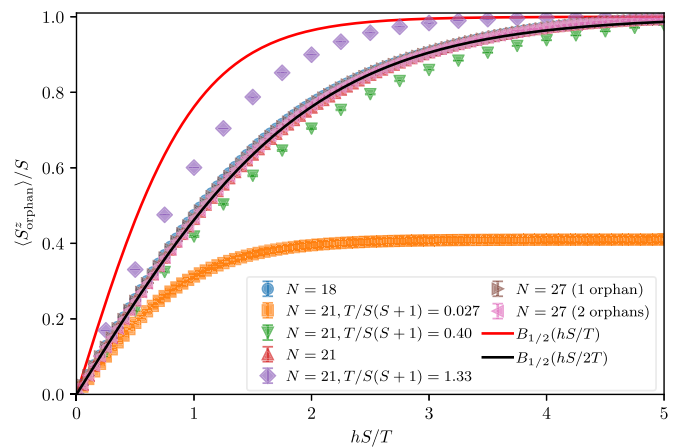


FIG. 9. Scaled orphan magnetization curve $\langle S_{\text{orphan}}^z \rangle / S$ as a function of scaled applied field hS/T , for various $S = 1/2$ kagome samples. For the 27-site kagome sample, we consider the case with two equivalent orphan spins. The temperature is $T/S(S+1) = 0.53$, unless specified in the legend. Also shown are the expected Brillouin functions for spin $S = 1/2$ at temperature T in field h and $h/2$.

Fig. 9 for a different set of lattice sizes where the adherence to the half-field Brillouin function is consistent for different samples with the same temperature scale. An interesting feature to note here is the behavior of the orphan impurity complexes in the 27-site sample with two such complexes. The screening cloud appears to be highly local as each of the two orphan spins responds exactly as a lattice with only one orphan spin. Furthermore, we find a plateau at low temperatures in the orphan response $\langle S_{\text{orphan}}^z \rangle$ as well as an approach to its saturation value through a series of plateaus at higher fields (not shown in Fig. 9). This is due to the discrete nature of the finite-size spectrum on such a small lattice (and at such low temperature), and it appears without any relationship to other well-known quantized plateaus that exist in the clean case [54–57].

The field dependence discussed above only appears for a particular temperature range which is controlled by thermal and quantum correlations. At high temperatures, the thermal correlation length is too short for the texture to survive, and at low temperatures the quantum correlation length is too long for the classical orphan description to work. It was noted in Ref. [23] that in the classical case, the expectation that the orphan texture in the SCGO bilayer provides exactly $h/2$ shielding works at temperatures below $T/S^2 \approx 0.2$. In the case of the kagome lattice, the classical results presented in the Appendix indicate that the orphan physics is slightly less stable to temperature (see Fig. 14) and we must thus expect a lower T/S^2 bound. This sets an approximate upper bound of temperature congruent with orphan physics for the quantum case as well for large spin- S .

To make a more quantitative prediction for this temperature range, we define the integrated square of the difference between the numerical data obtained with the typicality method and the expected form of the field response of the orphan. Considering the analytical Brillouin function for spin- S in magnetic field $h/2$, we compute the

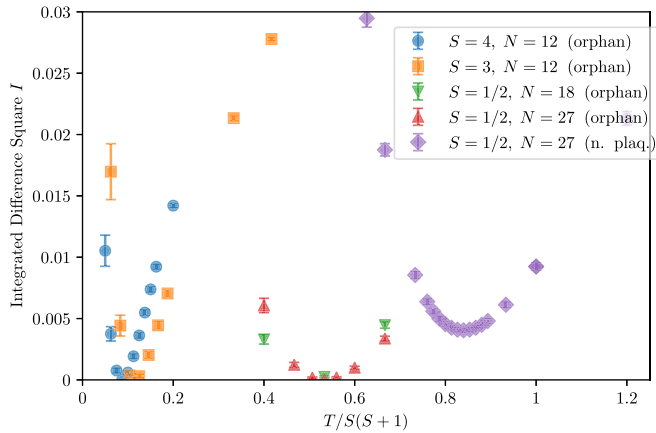


FIG. 10. Integrated difference square between the orphan magnetization curve and the half-field Brillouin function, as defined in Eq. (2), for different values of S and as a function of scaled temperature $T/S(S+1)$.

integral

$$I = \int dh [\langle S_{\text{orphan}}^z \rangle(h, T) - B_S(h/2, T)]^2, \quad (2)$$

where T is fixed. This quantity approaches zero only when the data fit the function to high accuracy in the window defined above. For numerical convenience, we define the integral to run from $h = 0$ to an h satisfying $B_{1/2}(hS/2T) = 0.9$. We have checked that this does not affect the conclusions.

We show results for the quantum case in Fig. 10 for $S = 3$ and 4 on the 12-site lattice with an orphan spin, along with $S = 1/2$ results on larger lattices. For all spin values, we find a temperature range where the data are extremely close to the half-field Brillouin function. This region can also be estimated directly from Fig. 5 by comparing the susceptibility with the expected value for the orphan defect. The deviations from orphan behavior at high temperatures arise from the same thermal fluctuations that melt orphan defects for the classical case, whereas the deviations at low temperatures arise from strong quantum fluctuations expected to render the spin-liquid description inapplicable. We chose in Figs. 8 and 9 the temperature close to the minima of I for $S = 4$ and $1/2$, respectively, but let us emphasize that displaying data at temperatures corresponding to values of $I \lesssim 0.01$ (respectively $I \lesssim 0.002$) would result in curves that would not be distinguishable for $S = 4$ (respectively $S = 1/2$) on the scale of Figs. 8 and 9. Based on the numerical evidence provided in Fig. 10, this leaves a fair range of temperatures where the orphan physics could be probed experimentally with local probes, for instance.

As can be noted furthermore in Fig. 10, there is no significant difference between 18- and 27-site samples for $S = 1/2$, implying that the orphan shielding is fairly local (as also expected from Refs. [23,24]). We also compare to the case in which the two impurities are on neighboring plaquettes to show that a strong $h/2$ shielding does not occur for any temperature range in this case. Although there is a minimum in the integrated difference square measure, the values at the minimum are significantly larger than corresponding values in cases in which orphan spins are present. The corresponding

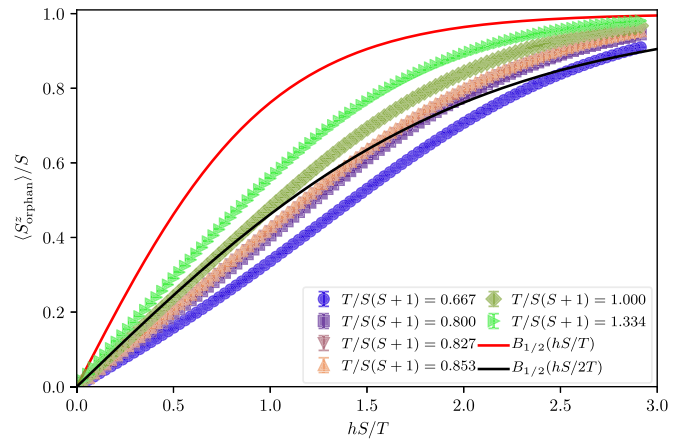


FIG. 11. Scaled orphan magnetization curve for an $S = 1/2$ 27-site lattice with neighboring plaquette impurities [Fig. 12(c)], where the points are shown for the range of hS/T used for the integrated difference.

magnetization curves are also quite distinct from the half-field Brillouin function (as seen in Fig. 11).

C. Local susceptibility distribution for doped $S = 1/2$ kagome systems

To make connections with possible experimental detection of orphan physics using NMR, we develop in this section a crude estimate for the distribution of local susceptibilities on large kagome samples for the case $S = 1/2$.

The procedure we consider is as follows. We work with a large lattice with $3 \times 300 \times 300 = 270\,000$ sites to be representative of the thermodynamic limit. On this lattice, we randomly pick sites to host a nonmagnetic impurity with probability 0.1. This nonmagnetic impurity doping fraction of 10% is chosen to ensure that we get a sizable number of orphans. The choice of temperature is guided by Fig. 9, where we see that $T/S(S+1) = 0.53$ (or $T = 0.4$) yields a good agreement with the orphan picture. At this temperature, we study a range of impurity patterns on the 27-site sample and find that only certain impurity patterns produce a local susceptibility that differs significantly from that of the pure system. Using this information, we find in particular that there are only six patterns that are relevant for sites that host a magnetic ion, some of which are presented pictorially in Fig. 12. The motivation to create this simple division is driven by the observation that for a temperature $T = 0.4$, quantum correlations are quite weak and the impurities do not influence significantly the sites that are separated by more than one bond, confirming that the physics is very local. In increasing order of probabilities of occurrence and together with a description of their magnetic response, these six patterns are as follows:

P1. All four neighbors of the ion are nonmagnetic impurities. This implies that the spin is completely decoupled from the lattice, and acts as a free spin $S = 1/2$.

P2. Three neighbors are nonmagnetic impurities: this is the situation in which an orphan spin has an additional nonmagnetic impurity next to it [see Fig. 12(a)]. We find that the response of this spin is only slightly stronger than that of the orphan spin.

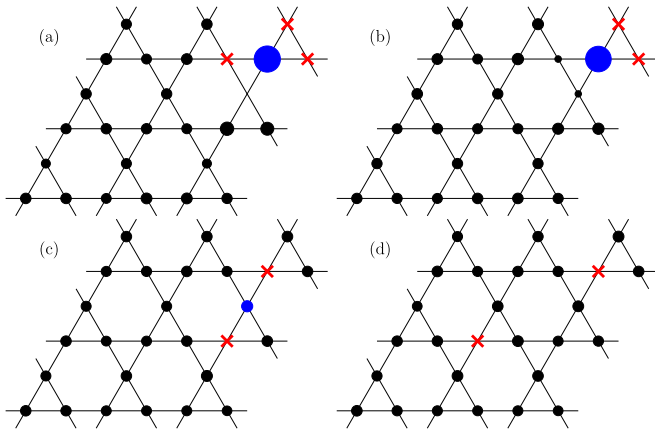


FIG. 12. Kagome 27-site samples showing the various nonmagnetic impurities (represented as red crosses) pattern considered for $S = 1/2$ experimental predictions (see text): (a) triple defect, (b) orphan spin, (c) impurities on neighboring plaquettes, and (d) two single impurities sufficiently separated. The case of two maximally separated orphans is the same as (d) with orphans in the locations of the crosses and the impurities in the triangle right of the orphan. The cases with all or no neighbors being impurities are not represented for simplicity. The radii of the circles are proportional to the value of the local susceptibility χ_{loc} at that site, at $T = 0.4$. Some sites may appear empty as the radius is too small to be visible.

P3. Two neighbors are nonmagnetic impurities [Fig. 12(b)]. This is the orphan spin, the response of which has been detailed earlier in this section.

P4. Two neighbors are nonmagnetic impurities on neighboring plaquettes but do not form an orphan [see Fig. 12(c)]. This has a response that is slightly stronger than the pure case.

P5. Only one neighbor is a nonmagnetic impurity [Fig. 12(d), which displays two of these cases]. We find also that this situation behaves similarly to the pure case with a slightly stronger response.

P6. No impurities are in the nearest neighbors. The response is well approximated by the pure case.

The six cases mentioned above lead to six peaks in the local susceptibility distribution $P(\chi_{loc})$, as displayed in the middle panel of Fig. 13 and ranked right to left (the free spin has obviously the largest local susceptibility). Given the very similar responses, it might be hard to distinguish the three leftmost peaks which are likely to form a main broad peak and correspond to the pure case as well as few impurity nonorphan physics. Note that in these cases, the impurity susceptibility is smaller (larger) than the pure one at low (high) temperature, in agreement with recent series expansion results [58]. The orphan physics is manifested through the presence of a secondary peak (where the cases *P2* and *P3* might also be hard to resolve). While this secondary peak is only about 2% of the main peak in strength, it is well separated from it, which gives hope for possible experimental detection. Also shown in Fig. 13 are results for $T = 0.2$ and 0.6 , which show the variation of the histogram with slight variations of the temperature away from the temperature ($T = 0.4$) that best fits the orphan picture. For $T = 0.2$, the quantum correlations may be too strong for the approximations *P1*–*P6* to strictly apply.

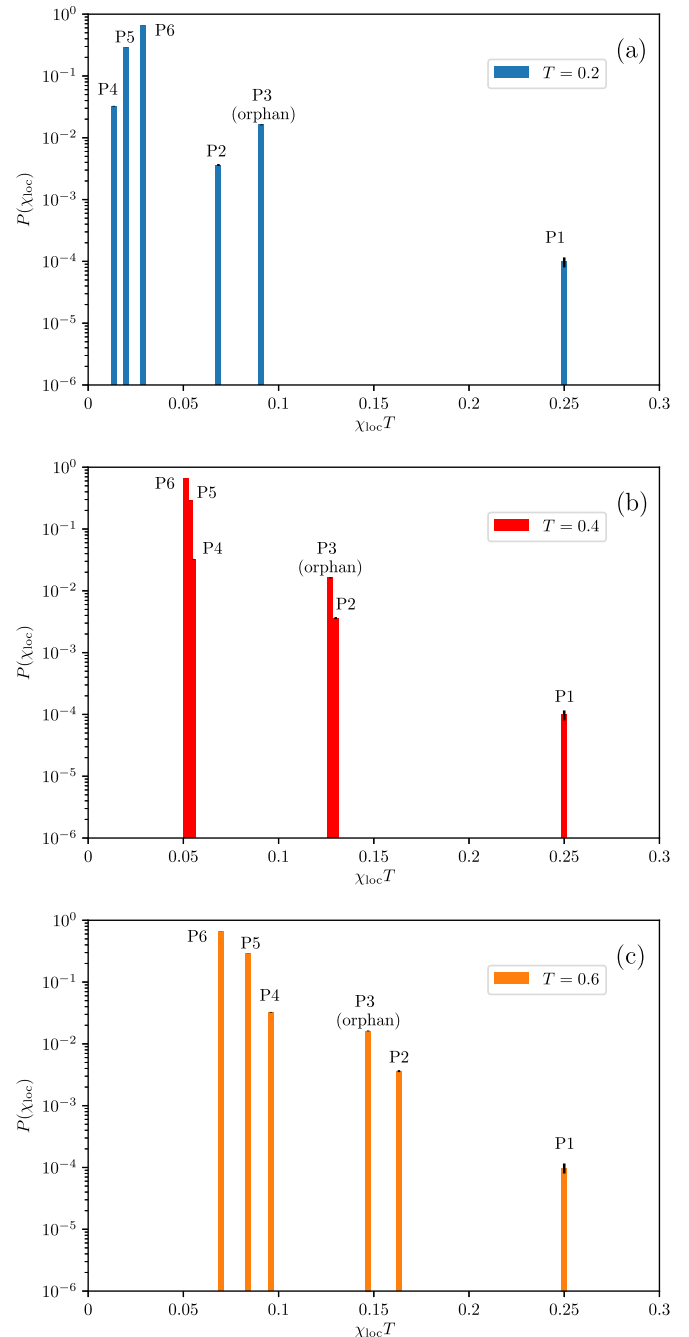


FIG. 13. The probabilities of occurrence of local susceptibilities in a 270 000-site lattice for $S = 1/2$ and $T = 0.2, 0.4,$ and 0.6 from top (a) to bottom (c). Note that the horizontal axis is scaled by T .

IV. CONCLUSIONS

In this work, we have investigated whether and how the physics of half-orphans, originally described using a classical theory, survives quantum effects and leads to clearly identifiable signatures in the response of quantum spin- S Heisenberg antiferromagnets on the kagome lattice when nearest-neighbor nonmagnetic impurities are present. We found that orphan-specific signatures are evident in local susceptibility data in an intermediate temperature range. We also found that the classical predictions for the screening cloud

around an orphan spin are justified in the quantum case. Indeed, the resulting spin texture is a more robust signature than the local susceptibility of the orphan spin itself, and it appears to provide a window to orphan physics even in the $S = 1/2$ case. Another striking result, for samples with a single orphan, is the strong dependence of the ground-state spin quantum number on the spin- S of the local moment itself. In complete agreement with the classical expectation, we found that the $S \geq 2$ kagome antiferromagnet with an orphan impurity complex has a ground-state spin, which is the nearest (half-)integer to $S/2$ allowed in most cases. Finally, we also presented experimental predictions for NMR Knight shifts on $S = 1/2$ kagome systems doped with nonmagnetic impurities, which point to the possibility of observing the enhanced orphan-induced magnetic response through a small, but resolvable, secondary peak.

In the appropriate temperature regime corresponding to spin-liquid behavior, these classical results on half-orphan spins are also expected to apply *mutatis mutandis* to other corner-sharing lattices such as the pyrochlore. Our results, taken in conjunction with this expectation, therefore provide strong motivation for other related studies. For instance, one follow-up suggested by our work is to consider whether the nonzero ground-state spin quantum number that we find in samples with an orphan impurity complex is also present for the Heisenberg model with sufficiently large spin- S on other corner-sharing lattices, for which the original $T = 0$ arguments go through unchanged. We hope to report on this in the near future.

A noteworthy feature of the orphan-induced spin texture studied here is that it appears to be a very local feature that exists in an intermediate temperature window, and this feature seems largely independent of the nature of the ground state, whose character can vary with the spin value S . For example, the Heisenberg kagome antiferromagnet with spin-1/2 has a ground state that is nonmagnetic, but the precise nature of this spin liquid (gapless versus gapped) is still debated [59–66]; in the spin-1 case, the ground state is also nonmagnetic, although whether it breaks lattice symmetries [67,68] or not [69] is still a matter of debate; for larger values of S , spin-wave analysis, coupled-cluster, or series expansion methods point to an ordered phase [70–72], while a large- N analysis, which generalizes the symmetry from $SU(2)$ to a larger symmetry group, leads to a nonmagnetic state [73].

It would be worth understanding how to incorporate the quantum orphan features found in our work in various effective field theories for these putative ground states [34]. Indeed, preliminary results suggest that some signatures of orphan physics are already present when samples with an orphan impurity complex are studied using relatively crude extensions of variational treatments inspired by such effective field theories. It would also be interesting to complement our study of quantum half-orphans by series expansion methods; this may be particularly fruitful since the textures induced by the orphans are relatively compact in the temperature range of their existence.

ACKNOWLEDGMENTS

We thank Ph. Mendels and L. Messio for discussions, and A. Wietek for useful insights about the typicality method.

K.D. would like to gratefully acknowledge earlier collaborations on closely related topics with R. Moessner, A. Sen, and S. Sanyal, which provided part of the motivation for this work. This work benefited from the support of the project LINK ANR-18-CE30-0022-04 of the French National Research Agency (ANR). We acknowledge the use of HPC resources from CALMIP (Grants No. 2019-P0677 and No. 2020-P0677) and GENCI (Grant No. x2020050225). We use the libraries ITensor for DMRG simulations [37], and PETSc [74,75] and SLEPc [76,77] for the typicality computations. We gratefully thank J. Roman for improving the Krylov method implementation in SLEPc to further ease typicality computations.

APPENDIX: CLASSICAL ORPHAN PHYSICS ON THE KAGOME LATTICE

In this Appendix, we expand on our introductory remarks on orphan spins on corner-sharing lattices and their main signatures in the finite-temperature properties of *classical* frustrated magnets, with particular emphasis on the kagome antiferromagnet of interest to us here. To this end, we consider in this Appendix classical spins S (vectors of magnitude $|S|$), coupled by a bilinear Heisenberg interaction on a network of corner-sharing simplices. For nearest-neighbor interactions, the Hamiltonian can be rewritten in terms of frustrated plaquette terms [19,22]. We have

$$H = \sum_{\langle i,j \rangle} \vec{S}_i \cdot \vec{S}_j = \frac{1}{2} \sum_p \left(\sum_{i \in p} \vec{S}_i \right)^2 + c, \quad (\text{A1})$$

where p labels plaquettes in the lattice. This is true for kagome and pyrochlore and pyrochlore-slab structures, and other structures where all pairs of spin within a plaquette are interacting.

The Hamiltonian written in plaquette language is minimized by setting $\sum_{i \in p} \vec{S}_i = 0$ for all plaquettes [22]. Replacing spins by nonmagnetic impurities reduces the number of spins participating in a plaquette term, but the energetic constraint can still be satisfied as long as there is more than one spin in a plaquette. The orphan spin situation illustrated in Fig. 1(a) corresponds to the case in which only one spin is left after substitution with nonmagnetic impurities.

As the orphan spin is released from the constraints coming from one plaquette (triangle for the kagome lattice), one expects that this spin remains “partially free” in some sense. As summarized in the Introduction, this expectation found a precise expression in the idea of a half-orphan degree of freedom in the work of Henley, and of Moessner and Berlinsky [19,22]. The detailed characterization of the response [23] indicates that the orphan behaves as a spin S object that sees an external field $h/2$ when an external field of h is applied. This paramagnetic response of the lone spin is partially screened by the net diamagnetic response of the surrounding spin texture, leading to a net low-temperature susceptibility identical to that of a spin $S/2$, as befits the response of an emergent half-orphan degree of freedom which behaves like a net spin- $S/2$ particle smeared across a few lattice spacings around the orphan [23].

For the specific case of the kagome lattice, there is a caveat: The classical spin liquid at intermediate temperatures gives

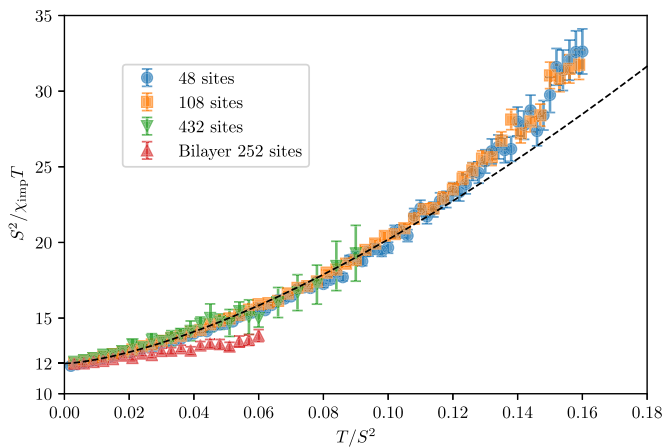


FIG. 14. Difference in the susceptibility between a sample with a single orphan complex and a sample with no impurities, $\chi_{\text{imp}} = \chi_{\text{tot}}^{\text{orphan}} - \chi_{\text{tot}}^{\text{pure}}$, as a function of temperature for the classical Heisenberg model on a kagome lattices of different sizes. A fit to the form $12 + aT^b$ at low temperature is also displayed. A comparison with the bilayer system shows that the orphan signature is stronger in the latter.

way at low enough temperature to a weakly ordered coplanar state of the classical Heisenberg model, where the coplanarity is itself a symmetry-breaking crossover phenomenon that occurs at $T^* \sim 10^{-3}JS^2$, and the subsequent entropically driven choice of a coplanar ordered state by anharmonic fluctuations only becomes apparent at even lower temperatures [28–30]. The smallness of T^* is fortuitous from the point of view of orphan physics: In the very broad temperature regime $T^* \ll T \ll JS^2$ in which there is spin liquid behavior, we expect a pair of vacancies on the same triangle to again nucleate an emergent half-orphan degree of freedom. Below, we confirm via classical Monte Carlo simulations that this is indeed true, although the temperature window in which half-orphan physics is well-established classically is seen to be smaller compared to the pyrochlore-slab lattice [23].

Reference [23] showed in the pyrochlore-slab magnet that the difference, denoted χ_{imp} in Ref. [23], of the total magnetic susceptibility χ_{tot} between a pure sample (with no impurities) and an otherwise pure sample with two nearest-neighbor nonmagnetic impurities (thus creating a single orphan) indeed corresponds to the response of a free spin of length $S/2$. As $\chi = S^2/(3T)$ for a single free spin, we should analogously expect to see at low temperatures a difference of the form $\chi_{\text{imp}} = \chi_{\text{tot}}^{\text{orphan}} - \chi_{\text{tot}}^{\text{pure}} = S^2/(12T)$ on the kagome lattice at intermediate temperatures well above the extremely low-temperature crossover to coplanar ordering, but well below the temperature scale set by JS^2 .

We have computed this difference χ_{imp} for several kagome samples using classical Monte Carlo simulations and standard

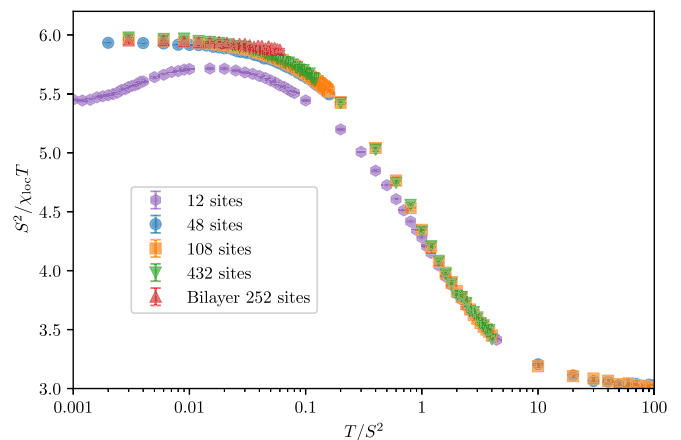


FIG. 15. Local susceptibility of the classical Heisenberg model on various samples sizes of the kagome lattice and bilayer, as a function of temperature.

METROPOLIS, Wolff cluster, and overrelaxation [78] updates to ensure ergodicity. Our results are displayed in Fig. 14, where we plot $S^2/(\chi_{\text{imp}}T)$ as a function of T to check the dependence with temperature in a clear manner. Data at the lower end of our temperature range converge to the expected constant 12, and we find a size-independent and smooth deviation away from this result. For the sake of completeness, we also reproduced the results of Ref. [23] for the bilayer with 252 sites, where we find the approach to the $T = 0$ limit to be even flatter.

The local susceptibility $\chi_{\text{loc}} = \langle S_{\text{orphan}}^z S_{\text{total}}^z \rangle / T$ should reflect that the orphan spin behaves as a free spin of length S in a magnetic field of strength $h/2$ (where h is the applied external field). This is expected due to the screening of the magnetic field by the neighbors of the orphan spin [24]. In the low-field linear regime, we thus expect $S^2/\chi_{\text{loc}}T = 6$ at sufficiently low but not-too-low temperature. Our Monte Carlo simulations (Fig. 15) are in good agreement with this expectation at low temperatures, with an approximately size-independent peel-off toward the high-temperature result of a free spin- S at temperature T : the data once again displayed as $S^2/(\chi_{\text{loc}}T)$ clearly exhibit a crossover from the value 6 (obtained for spin- $S/2$) at low-temperature to the high-temperature spin- S value 3. Figure 15 also represents data for the small-sized cluster of 12 sites, which is shown to be already close to the thermodynamic limit (with at most a difference less than 10%). This particular 12-site sample [which is represented in Fig. 1(a), along with the location of impurities and the orphan spin] is useful to compare with the quantum simulations reported in the main text, as we are limited to small sizes in our studies of the quantum problem.

- [1] L. Savary and L. Balents, Quantum spin liquids: A review, *Rep. Prog. Phys.* **80**, 016502 (2016).
 [2] C. Castelnovo, R. Moessner, and S. L. Sondhi, Magnetic monopoles in spin ice, *Nature (London)* **451**, 42 (2008).

- [3] A. Kitaev, Anyons in an exactly solved model and beyond, *Ann. Phys.* **321**, 2 (2006).
 [4] D. Poilblanc, A. Läuchli, M. Mambrini, and F. Mila, Spinon deconfinement in doped frustrated quantum antiferromagnets, *Phys. Rev. B* **73**, 100403(R) (2006).

- [5] A. Läuchli and D. Poilblanc, Spin-Charge Separation in Two-Dimensional Frustrated Quantum Magnets, *Phys. Rev. Lett.* **92**, 236404 (2004).
- [6] H. Alloul, J. Bobroff, M. Gabay, and P. J. Hirschfeld, Defects in correlated metals and superconductors, *Rev. Mod. Phys.* **81**, 45 (2009).
- [7] G. B. Martins, M. Laukamp, J. Riera, and E. Dagotto, Local Enhancement of Antiferromagnetic Correlations by Nonmagnetic Impurities, *Phys. Rev. Lett.* **78**, 3563 (1997).
- [8] R. K. Kaul, R. G. Melko, M. A. Metlitski, and S. Sachdev, Imaging Bond Order Near Nonmagnetic Impurities in Square-Lattice Antiferromagnets, *Phys. Rev. Lett.* **101**, 187206 (2008).
- [9] S. Sachdev and M. Vojta, Quantum impurity in an antiferromagnet: Nonlinear sigma model theory, *Phys. Rev. B* **68**, 064419 (2003).
- [10] K. H. Höglund, A. W. Sandvik, and S. Sachdev, Impurity Induced Spin Texture in Quantum Critical 2D Antiferromagnets, *Phys. Rev. Lett.* **98**, 087203 (2007).
- [11] S. Haravifard, S. R. Dunsiger, S. El Shawish, B. D. Gaulin, H. A. Dabkowska, M. T. F. Telling, T. G. Perring, and J. Bonča, In-Gap Spin Excitations and Finite Triplet Lifetimes in the Dilute Singlet Ground State System $\text{SrCu}_{2-x}\text{Mg}_x(\text{BO}_3)_2$, *Phys. Rev. Lett.* **97**, 247206 (2006).
- [12] M. Yoshida, H. Kobayashi, I. Yamauchi, M. Takigawa, S. Capponi, D. Poilblanc, F. Mila, K. Kudo, Y. Koike, and N. Kobayashi, Real Space Imaging of Spin Polarons in Zn-Doped $\text{SrCu}_2(\text{BO}_3)_2$, *Phys. Rev. Lett.* **114**, 056402 (2015).
- [13] F. Tedoldi, R. Santachiara, and M. Horvatić, ^{89}Y NMR Imaging of the Staggered Magnetization in the Doped Haldane Chain $\text{Y}_2\text{BaNi}_{1-x}\text{Mg}_x\text{O}_5$, *Phys. Rev. Lett.* **83**, 412 (1999).
- [14] A. Olariu, P. Mendels, F. Bert, F. Duc, J. C. Trombe, M. A. de Vries, and A. Harrison, ^{17}O NMR Study of the Intrinsic Magnetic Susceptibility and Spin Dynamics of the Quantum Kagome Antiferromagnet $\text{ZnCu}_3(\text{OH})_6\text{Cl}_2$, *Phys. Rev. Lett.* **100**, 087202 (2008).
- [15] J.-X. Yin, N. Shumiya, Y. Jiang, H. Zhou, G. Macam, H. O. M. Sura, S. S. Zhang, Z.-J. Cheng, Z. Guguchia, Y. Li *et al.*, Spin-orbit quantum impurity in a topological magnet, *Nat. Commun.* **11**, 1 (2020).
- [16] X. Obradors, A. Labarta, A. Isalgué, J. Tejada, J. Rodriguez, and M. Pernet, Magnetic frustration and lattice dimensionality in $\text{SrCr}_8\text{Ga}_4\text{O}_{19}$, *Solid State Commun.* **65**, 189 (1988).
- [17] A. P. Ramirez, G. P. Espinosa, and A. S. Cooper, Strong Frustration and Dilution-Enhanced Order in a Quasi-2D Spin Glass, *Phys. Rev. Lett.* **64**, 2070 (1990).
- [18] L. Limot, P. Mendels, G. Collin, C. Mondelli, B. Ouladdiaf, H. Mutka, N. Blanchard, and M. Mekata, Susceptibility and dilution effects of the kagomé bilayer geometrically frustrated network: A Ga NMR study of $\text{SrCr}_{9p}\text{Ga}_{12-9p}\text{O}_{19}$, *Phys. Rev. B* **65**, 144447 (2002).
- [19] R. Moessner and A. J. Berlinsky, Magnetic Susceptibility of Diluted Pyrochlore and $\text{SrCr}_{9-9x}\text{Ga}_{3+9x}\text{O}_{19}$ Antiferromagnets, *Phys. Rev. Lett.* **83**, 3293 (1999).
- [20] R. Moessner and J. T. Chalker, Properties of a Classical Spin Liquid: The Heisenberg Pyrochlore Antiferromagnet, *Phys. Rev. Lett.* **80**, 2929 (1998).
- [21] P. Schiffer and I. Daruka, Two-population model for anomalous low-temperature magnetism in geometrically frustrated magnets, *Phys. Rev. B* **56**, 13712 (1997).
- [22] C. L. Henley, Effective Hamiltonians and dilution effects in kagome and related anti-ferromagnets, *Can. J. Phys.* **79**, 1307 (2001).
- [23] A. Sen, K. Damle, and R. Moessner, Fractional Spin Textures in the Frustrated Magnet $\text{SrCr}_{9p}\text{Ga}_{12-9p}\text{O}_{19}$, *Phys. Rev. Lett.* **106**, 127203 (2011).
- [24] A. Sen, K. Damle, and R. Moessner, Vacancy-induced spin textures and their interactions in a classical spin liquid, *Phys. Rev. B* **86**, 205134 (2012).
- [25] D. Bono, P. Mendels, G. Collin, N. Blanchard, F. Bert, A. Amato, C. Baines, and A. D. Hillier, μSR Study of the Quantum Dynamics in the Frustrated $s = \frac{3}{2}$ kagomé bilayers, *Phys. Rev. Lett.* **93**, 187201 (2004).
- [26] P. Mendels and F. Bert, Quantum kagome antiferromagnet: $\text{ZnCu}_3(\text{OH})_6\text{Cl}_2$, *J. Phys.: Conf. Ser.* **320**, 012004 (2011).
- [27] P. Khuntia, M. Velazquez, Q. Barthélemy, F. Bert, E. Kermarrec, A. Legros, B. Bernu, L. Messio, A. Zorko, and P. Mendels, Gapless ground state in the archetypal quantum kagome antiferromagnet $\text{ZnCu}_3(\text{OH})_6\text{Cl}_2$, *Nat. Phys.* **16**, 469 (2020).
- [28] G.-W. Chern and R. Moessner, Dipolar Order by Disorder in the Classical Heisenberg Antiferromagnet on the Kagome Lattice, *Phys. Rev. Lett.* **110**, 077201 (2013).
- [29] M. E. Zhitomirsky, Octupolar ordering of classical kagome antiferromagnets in two and three dimensions, *Phys. Rev. B* **78**, 094423 (2008).
- [30] D. A. Huse and A. D. Rutenberg, Classical antiferromagnets on the kagomé lattice, *Phys. Rev. B* **45**, 7536 (1992).
- [31] S. Dommange, M. Mambrini, B. Normand, and F. Mila, Static impurities in the $s = 1/2$ kagome lattice: Dimer freezing and mutual repulsion, *Phys. Rev. B* **68**, 224416 (2003).
- [32] A. Läuchli, S. Dommange, B. Normand, and F. Mila, Static impurities in the $s = \frac{3}{2}$ kagome lattice: Exact diagonalization calculations on small clusters, *Phys. Rev. B* **76**, 144413 (2007).
- [33] R. R. P. Singh, Valence Bond Glass Phase in Dilute Kagome Antiferromagnets, *Phys. Rev. Lett.* **104**, 177203 (2010).
- [34] K. Gregor and O. I. Motrunich, Nonmagnetic impurities in the spin-1/2 kagome antiferromagnet, *Phys. Rev. B* **77**, 184423 (2008).
- [35] S. R. White, Density Matrix Formulation for Quantum Renormalization Groups, *Phys. Rev. Lett.* **69**, 2863 (1992).
- [36] U. Schollwöck, The density-matrix renormalization group in the age of matrix product states, *Ann. Phys.* **326**, 96 (2011).
- [37] M. Fishman, S. R. White, and E. M. Stoudenmire, The ITensor software library for tensor network calculations, [arXiv:2007.14822](https://arxiv.org/abs/2007.14822) (available at <http://itensor.org>).
- [38] J. Jaklič and P. Prelovšek, Lanczos method for the calculation of finite-temperature quantities in correlated systems, *Phys. Rev. B* **49**, 5065(R) (1994).
- [39] A. Hams and H. De Raedt, Fast algorithm for finding the eigenvalue distribution of very large matrices, *Phys. Rev. E* **62**, 4365 (2000).
- [40] S. Goldstein, J. L. Lebowitz, R. Tumulka, and N. Zanghì, Canonical Typicality, *Phys. Rev. Lett.* **96**, 050403 (2006).
- [41] S. Popescu, A. Short, and A. Winter, Entanglement and the foundations of statistical mechanics, *Nat. Phys.* **2**, 754 (2006).
- [42] P. Reimann, Typicality for Generalized Microcanonical Ensembles, *Phys. Rev. Lett.* **99**, 160404 (2007).

- [43] S. Sugiura and A. Shimizu, Canonical Thermal Pure Quantum State, *Phys. Rev. Lett.* **111**, 010401 (2013).
- [44] S. Sugiura and A. Shimizu, Thermal Pure Quantum States at Finite Temperature, *Phys. Rev. Lett.* **108**, 240401 (2012).
- [45] T. Shimokawa and H. Kawamura, Finite-temperature crossover phenomenon in the $s = 1/2$ antiferromagnetic Heisenberg model on the kagome lattice, *J. Phys. Soc. Jpn.* **85**, 113702 (2016).
- [46] J. Schnack, J. Schulenburg, and J. Richter, Magnetism of the $n = 42$ kagome lattice antiferromagnet, *Phys. Rev. B* **98**, 094423 (2018).
- [47] A. Wietek, P. Corboz, S. Wessel, B. Normand, F. Mila, and A. Honecker, Thermodynamic properties of the Shastry-Sutherland model throughout the dimer-product phase, *Phys. Rev. Research* **1**, 033038 (2019).
- [48] P. Prelovšek and J. Kokalj, Similarity of thermodynamic properties of the Heisenberg model on triangular and kagome lattices, *Phys. Rev. B* **101**, 075105 (2020).
- [49] J. Schnack, J. Richter, and R. Steinigeweg, Accuracy of the finite-temperature Lanczos method compared to simple typicality-based estimates, *Phys. Rev. Research* **2**, 013186 (2020).
- [50] M. Aichhorn, M. Daghofer, H. G. Evertz, and W. von der Linden, Low-temperature Lanczos method for strongly correlated systems, *Phys. Rev. B* **67**, 161103(R) (2003).
- [51] Z. Hiroi, M. Hanawa, N. Kobayashi, M. Nohara, H. Takagi, Y. Kato, and M. Takigawa, Spin-1/2 kagomé-like lattice in volborthite $\text{Cu}_3\text{V}_2\text{O}_7(\text{OH}) \cdot 2\text{H}_2\text{O}$, *J. Phys. Soc. Jpn.* **70**, 3377 (2001).
- [52] P. Mendels, F. Bert, M. A. de Vries, A. Olariu, A. Harrison, F. Duc, J. C. Trombe, J. S. Lord, A. Amato, and C. Baines, Quantum Magnetism in the Paratacamite Family: Towards an Ideal Kagomé Lattice, *Phys. Rev. Lett.* **98**, 077204 (2007).
- [53] T. Arh, M. Gomilšek, P. Prelovšek, M. Pregelj, M. Klanjšek, A. Ozarowski, S. J. Clark, T. Lancaster, W. Sun, J.-X. Mi, and A. Zorko, Origin of Magnetic Ordering in a Structurally Perfect Quantum Kagome Antiferromagnet, *Phys. Rev. Lett.* **125**, 027203 (2020).
- [54] J. Schulenburg, A. Honecker, J. Schnack, J. Richter, and H.-J. Schmidt, Macroscopic Magnetization Jumps Due to Independent Magnons in Frustrated Quantum Spin Lattices, *Phys. Rev. Lett.* **88**, 167207 (2002).
- [55] D. C. Cabra, M. D. Grynberg, P. C. W. Holdsworth, A. Honecker, P. Pujol, J. Richter, D. Schmalfuß, and J. Schulenburg, Quantum kagomé antiferromagnet in a magnetic field: Low-lying nonmagnetic excitations versus valence-bond crystal order, *Phys. Rev. B* **71**, 144420 (2005).
- [56] S. Nishimoto, N. Shibata, and C. Hotta, Controlling frustrated liquids and solids with an applied field in a kagome Heisenberg antiferromagnet, *Nat. Commun.* **4**, 2287 (2013).
- [57] S. Capponi, O. Derzhko, A. Honecker, A. M. Läuchli, and J. Richter, Numerical study of magnetization plateaus in the spin- $1/2$ kagome Heisenberg antiferromagnet, *Phys. Rev. B* **88**, 144416 (2013).
- [58] B. Bernu, L. Pierre, K. Essafi, and L. Messio, Effect of perturbations on the kagome $S = 1/2$ antiferromagnet at all temperatures, *Phys. Rev. B* **101**, 140403(R) (2020).
- [59] H. C. Jiang, Z. Y. Weng, and D. N. Sheng, Density Matrix Renormalization Group Numerical Study of the Kagome Antiferromagnet, *Phys. Rev. Lett.* **101**, 117203 (2008).
- [60] G. Evenbly and G. Vidal, Frustrated Antiferromagnets with Entanglement Renormalization: Ground State of the Spin- $1/2$ Heisenberg Model on a Kagome Lattice, *Phys. Rev. Lett.* **104**, 187203 (2010).
- [61] S. Yan, D. A. Huse, and S. R. White, Spin-liquid ground state of the $s = 1/2$ kagome Heisenberg antiferromagnet, *Science* **332**, 1173 (2011).
- [62] S. Depenbrock, I. P. McCulloch, and U. Schollwöck, Nature of the Spin-Liquid Ground State of the $s = 1/2$ Heisenberg Model on the Kagome Lattice, *Phys. Rev. Lett.* **109**, 067201 (2012).
- [63] Y. Iqbal, F. Becca, S. Sorella, and D. Poilblanc, Gapless spin-liquid phase in the kagome spin- $1/2$ Heisenberg antiferromagnet, *Phys. Rev. B* **87**, 060405(R) (2013).
- [64] S. Capponi, V. R. Chandra, A. Auerbach, and M. Weinstein, p_6 chiral resonating valence bonds in the kagome antiferromagnet, *Phys. Rev. B* **87**, 161118(R) (2013).
- [65] Y.-C. He, M. P. Zaletel, M. Oshikawa, and F. Pollmann, Signatures of Dirac Cones in a DMRG Study of the Kagome Heisenberg Model, *Phys. Rev. X* **7**, 031020 (2017).
- [66] H. J. Liao, Z. Y. Xie, J. Chen, Z. Y. Liu, H. D. Xie, R. Z. Huang, B. Normand, and T. Xiang, Gapless Spin-Liquid Ground State in the $s = 1/2$ Kagome Antiferromagnet, *Phys. Rev. Lett.* **118**, 137202 (2017).
- [67] H. J. Changlani and A. M. Läuchli, Trimerized ground state of the spin-1 Heisenberg antiferromagnet on the kagome lattice, *Phys. Rev. B* **91**, 100407(R) (2015).
- [68] T. Liu, W. Li, A. Weichselbaum, J. von Delft, and G. Su, Simplex valence-bond crystal in the spin-1 kagome Heisenberg antiferromagnet, *Phys. Rev. B* **91**, 060403(R) (2015).
- [69] S. Nishimoto and M. Nakamura, Non-symmetry-breaking ground state of the $S = 1$ Heisenberg model on the kagome lattice, *Phys. Rev. B* **92**, 140412(R) (2015).
- [70] A. Chubukov, Order from Disorder in a Kagomé Antiferromagnet, *Phys. Rev. Lett.* **69**, 832 (1992).
- [71] O. Götze, D. J. J. Farnell, R. F. Bishop, P. H. Y. Li, and J. Richter, Heisenberg antiferromagnet on the kagome lattice with arbitrary spin: A higher-order coupled cluster treatment, *Phys. Rev. B* **84**, 224428 (2011).
- [72] J. Oitmaa and R. R. P. Singh, Competing orders in spin-1 and spin- $3/2$ XXZ kagome antiferromagnets: A series expansion study, *Phys. Rev. B* **93**, 014424 (2016).
- [73] S. Sachdev, Kagomé- and triangular-lattice Heisenberg antiferromagnets: Ordering from quantum fluctuations and quantum-disordered ground states with unconfined bosonic spinons, *Phys. Rev. B* **45**, 12377 (1992).
- [74] S. Balay, W. D. Gropp, L. C. McInnes, and B. F. Smith, Efficient management of parallelism in object oriented numerical software libraries, in *Modern Software Tools in Scientific Computing*, edited by E. Arge, A. M. Bruaset, and H. P. Langtangen (Birkhäuser, Boston, 1997), pp. 163–202.
- [75] S. Balay, S. Abhyankar, M. F. Adams, J. Brown, P. Brune, K. Buschelman, L. Dalcin, V. Eijkhout, W. D. Gropp, D. Kaushik, M. G. Knepley, L. C. McInnes, K. Rupp, B. F. Smith, S. Zampini, H. Zhang, and H. Zhang, PETSc Users Manual, Tech. Rep. ANL-95/11–Revision 3.8 (Argonne National Laboratory, 2017).

- [76] V. Hernandez, J. E. Roman, and V. Vidal, SLEPc: A scalable and flexible toolkit for the solution of eigenvalue problems, *ACM Trans. Math. Softw.* **31**, 351 (2005).
- [77] J. E. Roman, C. Campos, E. Romero, and A. Tomas, SLEPc Users Manual, Tech. Rep. DSIC-II/24/02–Revision 3.8 (D. Sistemes Informàtics i Computació, Universitat Politècnica de València, 2017).
- [78] L. W. Lee and A. P. Young, Large-scale Monte Carlo simulations of the isotropic three-dimensional Heisenberg spin glass, *Phys. Rev. B* **76**, 024405 (2007).